Journal of Biomechanics 111 (2020) 110001

Contents lists available at ScienceDirect

Journal of Biomechanics

journal homepage: www.elsevier.com/locate/jbiomech
www.JBiomech.com

From perviousness to permeability, modelling and measuring intra-thrombus flow in acute ischemic stroke

Nerea Arrarte Terreros [a,b,*], Manon L. Tolhuisen [a,b], Edwin Bennink [c], Hugo W.A.M. de Jong [d], Ludo F.M. Beenen [b], Charles B.L.M. Majoie [b], Ed van Bavel [a], Henk A. Marquering [a,b]

[a] Department of Biomedical Engineering and Physics, Amsterdam UMC, Location AMC, Amsterdam, the Netherlands
[b] Department of Radiology and Nuclear Medicine, Amsterdam UMC, Location AMC, Amsterdam, the Netherlands
[c] Image Science Institute, UMC Utrecht, Utrecht, the Netherlands
[d] Department of Radiology and Nuclear Medicine, UMC Utrecht, Utrecht, the Netherlands

ARTICLE INFO

Article history:
Accepted 14 August 2020

Keywords:
Blood flow quantification
Thrombus permeability
Dynamic CTA
Acute ischemic stroke

ABSTRACT

Thrombus permeability determines blood flow through the occluding thrombus in acute ischemic stroke (AIS) patients. The quantification of thrombus permeability is challenging since it cannot be directly measured nor derived from radiological imaging data. As a proxy of thrombus permeability, thrombus perviousness has been introduced, which assesses the amount of contrast agent that has penetrated the thrombus on single-phase computed tomography angiography (CTA). We present a method to assess thrombus permeability rather than perviousness. We follow a three-step approach: (1) we propose a theoretical channel-like structure model describing the thrombus morphology. Using Darcy's law, we provide an analytical description of the permeability for this model. According to the channel-like model, permeability depends on the number of channels in the thrombus, the radius of the occluded artery, and the void fraction representing the volume available for the blood to flow; (2) we measure intra-thrombus blood flow and velocity on dynamic CTA; and (3) we combine the analytical model with the dynamic CTA measurements to estimate thrombus permeability. Analysis of dynamic CTA data from 49 AIS patients showed that the median blood velocity in the thrombus was 0.58 (IQR 0.26–1.35) cm/s. The median flow within the thrombus was $3.48 \cdot 10^{-3}$ (IQR $1.71 \cdot 10^{-3}$–$9.21 \cdot 10^{-3}$) ml/s. Thrombus permeability was of the order of 10^{-3}–10^{-5} mm^2, depending on the number of channels in the thrombus. The channel-like thrombus model offers an intuitive way of modelling thrombus permeability, which can be of interest when studying the effect of thrombolytic drugs.

1. Introduction

An acute ischemic stroke (AIS) is caused when a thrombus severely occludes an intracranial artery, restricting blood supply to the brain. The deprivation of blood to the brain rapidly causes brain tissue ischemia, which requires immediate treatment. Currently, there are two kinds of treatment that aim at re-establishing intracranial perfusion: intra-venous thrombolysis (Modrau et al., 2007), which aims to dissolve the thrombus, and mechanical thrombectomy (Berkhemer et al., 2015), which aims to retrieve the thrombus from the vasculature. Despite the availability of two treatment options, still almost 2 out of 3 patients end up with poor functional outcome after treatment (Jansen et al., 2018).

The occluding thrombus is commonly formed by a fibrin fibre network trapping red blood cells (RBC), platelets and other blood constituents (Boeckh-Behrens et al., 2016; Marder et al., 2006). Thrombi vary in composition, age, and morphology (De Meyer et al., 2017), which results in a wide spectrum of thrombus characteristics that may affect treatment outcome. The quantification of thrombus characteristics opens the possibility of a more effective treatment design. For instance, thrombus friction properties have been shown to be related to thrombus composition (Gunning et al., 2018). The differences in friction between the thrombus and the vessel wall may suggest the use of a particular thrombectomy stent design.

Permeability is an important thrombus characteristic. Preclinical wound healing studies have shown that a thrombus can be porous and permeable (Brass et al., 2011). The permeability of a thrombus reflects the ability of blood to flow through the gaps between adjacent fibrin filaments, trapped platelets and RBC.

* Corresponding author.
E-mail address: n.arrarteterreros@amsterdamumc.nl (N. Arrarte Terreros).

https://doi.org/10.1016/j.jbiomech.2020.110001
0021-9290/

Permeability is related to porosity, but also to the shapes and connectivity of these pores, i.e. two media with same porosity can differ in permeability because of different pore shapes and connectivities. It has been suggested that thrombus permeability plays a major role in treatment outcome (Frölich et al., 2014; Santos et al., 2016a). Thrombus permeability may enhance the dissolution speed of thrombolytic drugs. Permeability increases the surface contact area of the drug with the thrombus, which can facilitate the dissolution of the fibrin network.

The quantification of thrombus permeability is challenging since it cannot be directly measured nor derived from radiological imaging data. As a proxy for thrombus permeability, thrombus perviousness has been introduced (Santos et al., 2016b). Perviousness assesses the amount of contrast agent that has penetrated the thrombus, by comparing density in computed tomography angiography (CTA) and non-contrast computed tomography (NCCT) images. Perviousness has been proven to be related with improved patient outcome. Among patients treated with thrombolytic drugs, patients who had complete recanalization had more pervious thrombi (Santos et al., 2016a). However, perviousness is quantified in single-time radiological images, which do not consider flow propagation through the thrombus; therefore, perviousness does not fully represent thrombus physical permeability (Frölich et al., 2014, 2013; Santos et al., 2016b). Dynamic CTA imaging records multiple single-time CTAs over time, which opens the possibility to determine the dynamics of blood flow through and in the vicinity of the thrombus, and overcome the time-dependency of single-time CT imaging.

In this study, we aim to use the contrast-flow information provided by dynamic CTA to assess thrombus permeability rather than perviousness. In order to quantify thrombus permeability, we combine measurements of intra-thrombus flow from dynamic CTA data of AIS patients and a theoretical model describing permeability. We focus on proximal middle cerebral artery (MCA) occlusions, as these occlusions are the most common anterior large vessel occlusions (Goyal et al., 2016).

2. Methods

To come to a comprehensive description of the thrombus permeability, we followed a three steps approach:

- Part I. We described thrombus permeability based on Darcy's law. We developed an analytical model based on analogy to electrical circuits that describes the relation between pressure drop over the occlusion, intra-thrombus flow and the occluded vessel resistance. We derived a channel-like thrombus model to determine the relation between the occluded vessel resistance and the permeability.
- Part II. We measured intra-thrombus flow on dynamic CTA.
- Part III. We combined the analytical model with the intra-thrombus flow measurements to provide estimations of the permeability. In addition, we presented patient-specific cases.

2.1. Part I: Permeability model

The contrast propagation observed in the dynamic CTA data suggested an advective transport of contrast rather than diffusive (Appendix A). Therefore, our model is based on a hydraulic permeability rather than a diffusive permeability.

Permeability, κ [m^2], can be analytically expressed using Darcy's law, which describes flow through a porous medium,

$$v = -\frac{\kappa}{\mu}\vec{\nabla}P, \tag{1}$$

where v is the fluid velocity, μ is the fluid viscosity, and $\vec{\nabla}P$ is the pressure gradient along the permeable medium. For an anisotropic medium, which is the most general case, permeability is a tensor. For a vessel occluding thrombus, we neglected the local flow directions through the porous medium and assumed the fluid flow to be predominantly axial, reducing Eq. (1) to its 1-dimensional equivalent. In addition, we assumed the thrombus to be homogenous. With these assumptions, thrombus permeability is defined as

$$\kappa_{thrombus} = \mu v_{blood}\frac{L_{thrombus}}{\Delta P_{thrombus}}, \tag{2}$$

where v_{blood} is the blood velocity in the thrombus, $L_{thrombus}$ is the thrombus length, and $\Delta P_{thrombus}$ is the pressure drop over the occlusion.

The thrombus length and the blood velocity were determined from dynamic CTA data. The pressure drop however cannot be derived from radiological imaging or peri-procedural data and an alternative approach was needed here.

2.1.1. Electrical circuit model

Circuit theory provides the relation between local pressures, flows and resistances in a network of vessels including the pressure drop over the thrombus. In this model, flow was assumed to be laminar and steady, and the effects of vessel compliance and blood inertia were neglected.

According to Ohm's law, the pressure drop over the occlusion, $\Delta P_{thrombus}$, is given by

$$\Delta P_{thrombus} = Q_{thrombus}R_{thrombus}, \tag{3}$$

where $Q_{thrombus}$ is the blood flow through the thrombus, and $R_{thrombus}$ is the vessel resistance due to the occlusion. Eq. (3) can be used to estimate the pressure drop over the thrombus, needed for the permeability quantification.

The flow can be estimated by assessing the intra-thrombus blood velocity, v_{blood}, and the open cross-sectional vessel area perpendicular to the blood direction, A_{open},

$$Q_{thrombus} = v_{blood}A_{open}. \tag{4}$$

Substituting the estimation for pressure drop and blood flow of Eqs. (3) and (4) in (2) leads to an expression for thrombus permeability,

$$\kappa_{thrombus} = \mu\frac{L_{thrombus}}{R_{thrombus}A_{open}}, \tag{5}$$

which only depends on the occluded vessel resistance and geometrical characteristics of the thrombus. The occluded vessel resistance, $R_{thrombus}$, cannot be estimated from the circuit model nor from dynamic CTA measurements.

2.1.2. Channel-like thrombus model

The thrombus resistance was estimated based on a parallel channel model. This model consisted of a cylindrical straight tube with N identical channels covering the thrombus length. The portion of the volume covered by the open channels is known as the void fraction, α. Fig. 1 shows a graphical representation of the channel-like thrombus model.

Poiseuille's law describes the resistance, R, of a straight cylindrical tube [4],

$$R = \frac{8\mu L}{\pi r^4}, \tag{6}$$

where μ is the fluid viscosity, L is the tube length, and r is the tube radius. According to the channel-like model, the thrombus resistance, $R_{thrombus}$, is given by the parallel resistance of N identical channels, R_{ch},

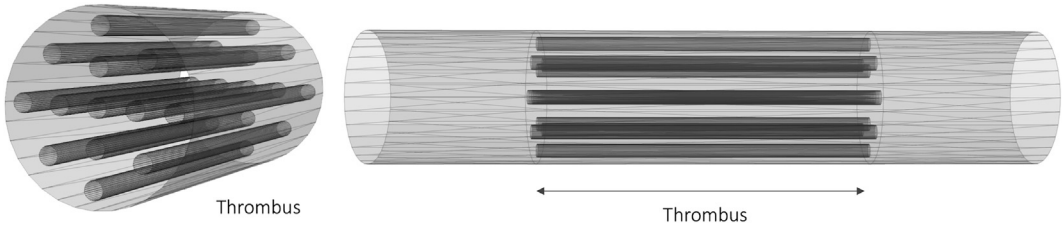

Fig. 1. Illustration of the channel-like thrombus model. Left: a schematic representation of a channel-like thrombus with 13 channels and 20% open volume ($\alpha = 0.2$). Right: the channel-like thrombus displayed on the left incorporated in a cylindrical tube modelling the vessel.

$$\frac{1}{R_{thrombus}} = \sum_{i=1}^{N} \frac{1}{R_{ch}} = \frac{N\pi r_{ch}^4}{8\mu L_{thrombus}} \tag{7}$$

where r_{ch} is the radius of a single channel. We derived a relation between the channel radius, r_{ch}, the MCA radius, r_{MCA}, and the void fraction. The volume of the channels and the total volume of the thrombus are related by

$$V_{channels} = \alpha V_{thrombus}. \tag{8}$$

The volume of the cylindrical channels is the sum of the volume of N single channels and therefore,

$$N\pi r_{ch}^2 L_{thrombus} = \alpha\pi r_{MCA}^2 L_{thrombus}. \tag{9}$$

Then,

$$r_{ch} = \sqrt{\frac{\alpha}{N}} r_{MCA}. \tag{10}$$

The thrombus resistance can be rewritten as

$$\frac{1}{R_{thrombus}} = \frac{\pi\alpha^2 r_{MCA}^4}{8N\mu L_{thrombus}}. \tag{11}$$

According to the channel-like model, the open cross-sectional vessel area perpendicular to the blood direction is the cross-sectional area of the channels, and therefore,

$$A_{open} = N\pi r_{ch}^2 = \alpha\pi r_{MCA}^2. \tag{12}$$

Introducing Eqs. (11) and (12) in the permeability Eq. (5) leads to a simple reformulation for the thrombus permeability,

$$\kappa_{thrombus} = \frac{\alpha r_{MCA}^2}{8N}. \tag{13}$$

In this formulation, permeability only depends on the radius of the MCA, the void fraction, and the number of channels.

The contact area of the thrombus is given by the contact area of the N open cylindrical channels,

$$A_{contact} = N2\pi r_{ch} L_{thrombus}. \tag{14}$$

Introducing Eq. (10) in (14) leads to

$$A_{contact} = \sqrt{N\alpha} 2\pi r_{MCA} L_{thrombus}. \tag{15}$$

It appears that the derived permeability, Eq. (13), is a simplified version of the Kozeny-Carman equation (Carman, 1939; Kozeny, 1927), assuming straight channels.

2.2. Part II: Dynamic CTA measurements

2.2.1. Data sets

In this study, we included image data of 49 patients from the Amsterdam UMC, (Amsterdam, the Netherlands) and the Dutch acute stroke trial (DUST) (Van Seeters et al., 2014). All patients had an ischemic stroke with a single occlusion in the MCA. For all 49 patients, dynamic CTA data were available (Supplementary Material, video 1). We additionally collected NCCT scans, if available. Typical resolution of the data was $\Delta x \cdot \Delta y \cdot \Delta z \cdot \Delta t$ = 0.391 mm · 0.391 mm · 0.8 mm · 2 s.

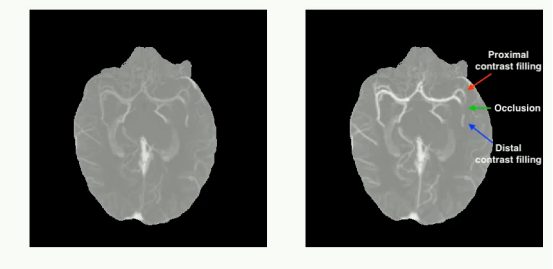

Video displaying a dynamic CTA scan of an AIS patient. Right: MIP of a dynamic CTA scan indicating the contrast filling proximal and distal to the thrombus (red and blue arrows, respectively), and the occlusion location on the left MCA (green arrow). Left: video displaying the contrast propagation on dynamic CTA. The video is a partial MIP so the occlusion is completely visible and contrast propagation can be followed through the arteries of interest. Contrast arrival to the occluded side is slower than to the contralateral side, especially distal to the occlusion. The scan consisted of 30 timeframes collected every 2 s. We displayed the most informative timeframes (5 to 25). The video displays one timeframe every 2 s to resemble the real acquisition time.

The Amsterdam UMC data were acquired using a Siemens Somaton Force and Siemens Somaton Definition AS scanners with a tube voltage of 70 kV. These dynamic CTA scans were source data from CT perfusion scans. The used convolution kernels were Hr36f and H20f. Details regarding the DUST image acquisition can be found in Van Seeters et al. (2014).

The image data were preprocessed. First, skull-stripping was applied. For the dynamic CTA data, each timeframe was aligned to the first timeframe using rigid registration. When NCCT scans were available, the NCCT and dynamic CTA scans were co-registered. Registration was performed using Elastix (Klein et al., 2010). The dynamic CTA data were filtered using a bilateral filter (Bennink et al., 2015). For 4 scans, this filtering was not sufficient, and an additional Butterworth filter was applied to remove high frequency noise in time.

We developed a MATLAB based Graphical User Interface (GUI) to perform the intra-thrombus flow measurements. The GUI allows visualizing dynamic CTA data and manually placing markers. We placed markers proximal, in, and distal to the thrombus following the vessel centerline (Fig. 2). To facilitate the positioning of the markers, temporal maximum intensity projection (t-MIP) maps were created.

We additionally placed three markers on the contralateral MCA, in the symmetrical positions corresponding to the beginning, the mid-point, and the end of the thrombus. These contralateral markers were needed for the quantification of the thrombus void fraction (Santos et al., 2016b). The total number of markers (mean and standard deviation) is reported in the results.

From each manually placed marker, the average intensity of a sphere with a 0.5 mm radius was recorded, to reduce the

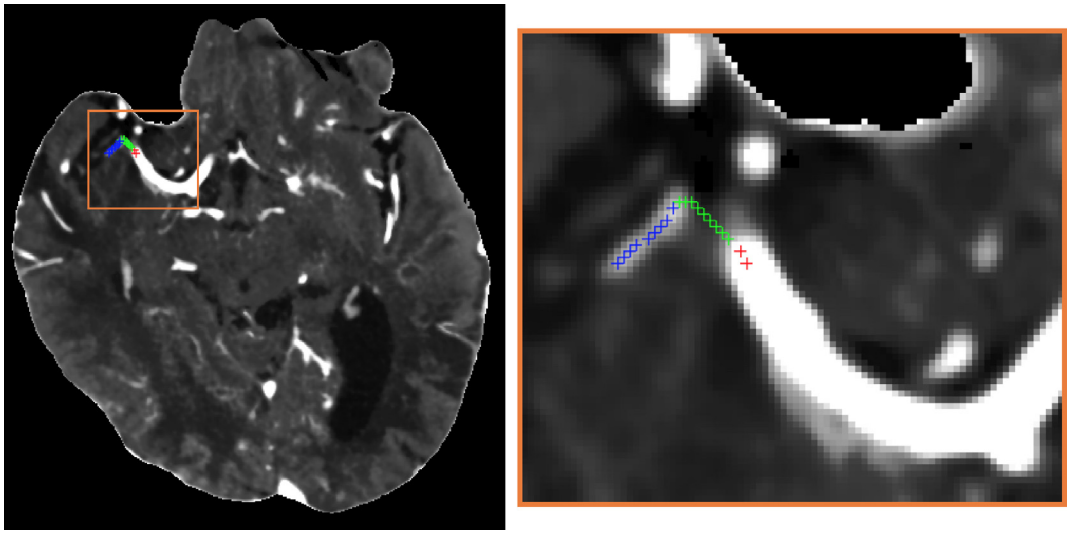

Fig. 2. Visualization of the markers on a temporal maximum intensity projection (t-MIP). Left: example of a t-MIP of a right middle cerebral artery (MCA) occlusion. Right: closer view of the occlusion shown on the left. Markers proximal, in, and distal to the thrombus are displayed in red, green, and blue, respectively.

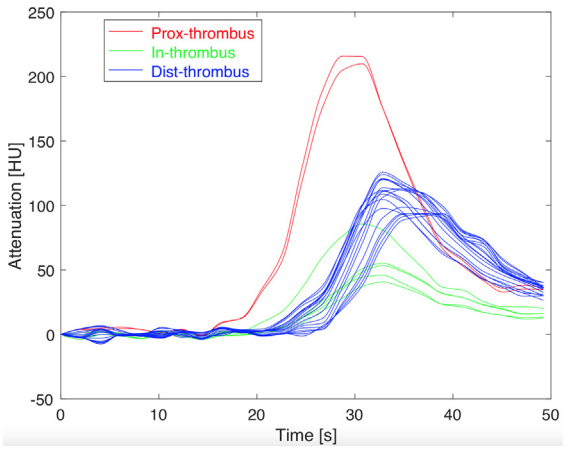

Fig. 3. Time attenuation curves (TACs). Contrast intensity attenuation [HU] over time [s] for markers placed proximal, in, and distal to the thrombus (red, green, and blue curves, respectively) on a dynamic CTA scan.

sampling-bias while ensuring that only MCA voxels were selected. From each such region of interest, the contrast intensity over time was measured and displayed as the time attenuation curves (TACs) shown in Fig. 3. The measured TACs were oversampled using shape-preserving piecewise cubic interpolation.

2.2.2. Flow measurements

Blood velocity, v_{blood}, was calculated from the dynamic CTA data on thrombus length, $L_{thrombus}$, and blood transit-time, TT_{blood},

$$v_{blood} = \frac{L_{thrombus}}{TT_{blood}}. \tag{16}$$

The thrombus length was determined by computing the Euclidean distance between adjacent markers. The blood transit-time is the time that blood spends traveling from the beginning to the end of the occlusion. Blood transit-time is determined using a cross-correlation of the proximal and distal TACs.

According to the channel-like model, the open cross-sectional area perpendicular to the flow is given by

$$A^{open}_{vessel} = \alpha \pi r^2_{MCA}. \tag{17}$$

The thrombus void fraction, α, is the fraction of the thrombus open to contrast filling on dynamic CTA. It was computed as the ratio of the mean contrast intensity in the thrombus to the mean contrast intensity in the contralateral side, similar to the method described in Santos et al. (2016b).

$$\alpha = \frac{\left(\langle I_{t-MIP}\rangle - \langle I_{tf_0}\rangle\right)_{thrombus}}{\left(\langle I_{t-MIP}\rangle - \langle I_{tf_0}\rangle\right)_{contralateral}}, \tag{18}$$

where $\langle I_{t-MIP}\rangle$ and $\langle I_{tf_0}\rangle$ are the mean contrast intensity of the t-MIP and the first timeframe of the dynamic CTA scan, respectively. For evenly distributed void space over length, α also holds for the cross-sectional area.

Then, equation (4) becomes

$$Q_{thrombus} = \frac{\alpha \pi r^2_{MCA} L_{thrombus}}{TT_{blood}}. \tag{19}$$

We studied the relation of thrombus length, blood transit-time, and intra-thrombus blood velocity with thrombus void fraction. The error quantification of these measurements can be found in the Appendix B.

2.3. Part III. Combining the permeability model and the flow measurements

We studied thrombus permeability in two ways. On the one hand, we studied permeability according to Darcy's law, Eq. (2). We used the median thrombus length and the range of velocities we measured on dynamic CTA. The pressure drop, which could not be measured, was set to be between 30 and 100 mmHg, based on the only study (as far as we are aware of) that has measured intracranially the pressure drop over the occlusion (Sorimachi et al., 2011). The viscosity of blood was set to 3 mPa·s (Elert, 2019). The effect of blood viscosity and thrombus length on permeability can be found in the Appendix C .

On the other hand, we studied permeability according to the channel-like thrombus model, Eq. (13). The void fraction range was taken from the dynamic CTA measurements. The MCA radius was fixed in this study and set to 0.11 cm (Davison et al., 2018). The number of channels had to be estimated and was set to be between 1 and 1000 channels (Appendix D). We also studied

how the thrombus contact area and the thrombus resistance scale with the channel number and void fraction, Eqs. (15) and (11), respectively. The effect of varying MCA radius can be found in the Appendix C.

3. Results

3.1. Dynamic CTA measurements

Thrombus measurements could be performed for all 49 patients. The average number of markers per patient was 32 ± 6. In some cases, the time resolution of the scans was insufficient to determine the transit-time. For the velocity and flow histograms, these cases were excluded (n = 5). All the measurements can be found in Fig. 4 and Table 1.

Scatterplots showing the relation between the measurements are shown in Fig. 5. The scatter plots of thrombus length and blood transit-time over thrombus void fraction show disperse distributions. For any void fraction, the velocities were low (below 10 cm/s).

Table 1
Median and Interquartile range (IQR) for thrombus length [cm], thrombus void fraction [-], blood transit-time [s], intra-thrombus blood velocity [cm/s] and intra-thrombus flow [ml/s].

	Median (IQR)
Thrombus length [cm]	1.47 (0.87–1.99)
Thrombus void fraction	0.19 (0.13–0.25)
Blood transit-time [s]	2.10 (0.78–3.98)
Blood velocity [cm/s]	0.58 (0.26–1.35)
Blood flow 10^{-3} [ml/s]	3.48 (1.71–9.21)

3.2. Combining the permeability model and the flow measurements

3.2.1. Darcy's law

The relation between pressure drop, blood velocity and permeability is displayed in Fig. 6, with permeability values of the order of 10^{-4}–10^{-5} mm^2. For the same cross-sectional area, higher velocities and smaller pressure drops lead to higher permeability.

3.2.2. Channel-like permeability

The relation between thrombus void fraction, number of channels and permeability is shown in Fig. 6, with permeability values ranging from 10^{-3} to 10^{-5} mm^2. The effect of the void fraction and the number of channels in the thrombus contact area and vessel resistance is displayed in Fig. 7. For a constant void fraction, fewer but wider channels resulted in smaller vessel resistance and higher permeability, but less contact area. For equal number of channels, larger void fraction results in more contact area, smaller vessel resistance, and higher permeability.

3.2.3. Case analysis

To illustrate our measures and calculations, we here present permeability estimations for two patients and the median patient in the study population (Table 2). Compared to the study population, patient I had a relatively short thrombus, high porosity, high blood velocity and large blood flow. Distal to the occlusion, anterograde flow was observed. Patient II had an average length thrombus, low porosity, long transit-times, high blood velocity and little blood flow. Distal to the occlusion, contrast transport was in the retrograde direction.

According to the presented channel-like thrombus model, for the same number of channels, patient I had lower thrombus resistance and a more permeable thrombus, compared to patient II (Fig. 8).

4. Discussion

We have presented a thrombus permeability model based on dynamic measurements and a hemodynamic analysis in patients with an AIS. The observed contrast agent propagation over time

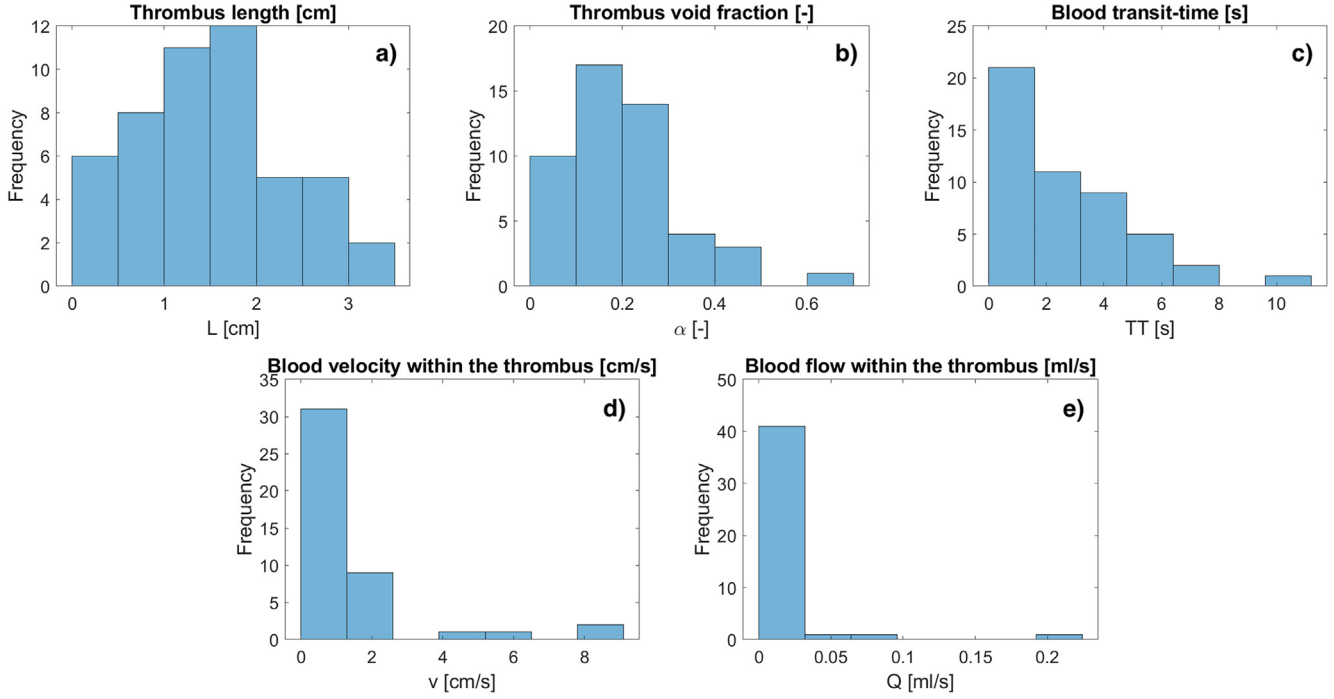

Fig. 4. Histograms of the performed dynamic CTA measurements. (a) Thrombus length [cm] histogram (n = 49). (b) Thrombus void fraction [-] histogram (n = 49). (c) Blood transit-time [s] histogram (n = 49) (d) Blood velocity within the thrombus [cm/s] histogram (n = 44). (e) Intra-thrombus flow [ml/s] histogram (n = 44).

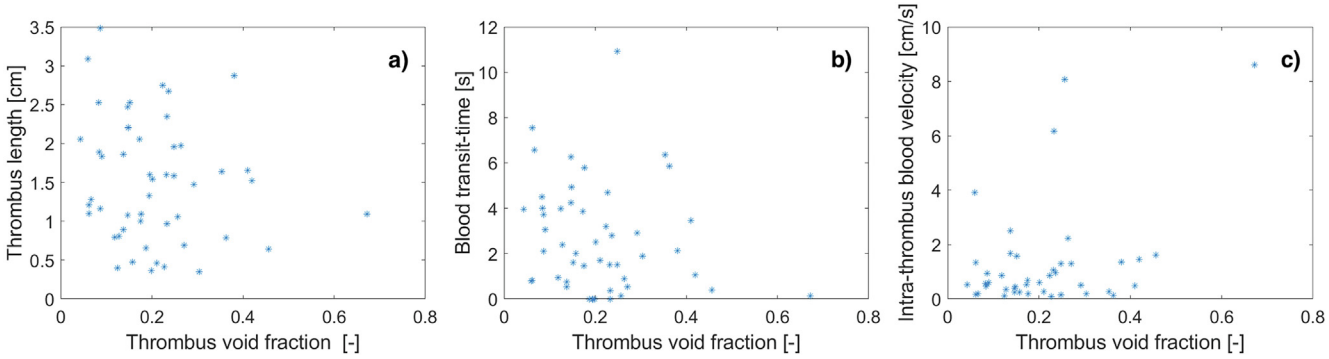

Fig. 5. Scatter plots showing the relation of (a) thrombus length [cm], (b) blood transit-time [s], and (c) intra-thrombus blood velocity [cm/s] with thrombus void fraction [-].

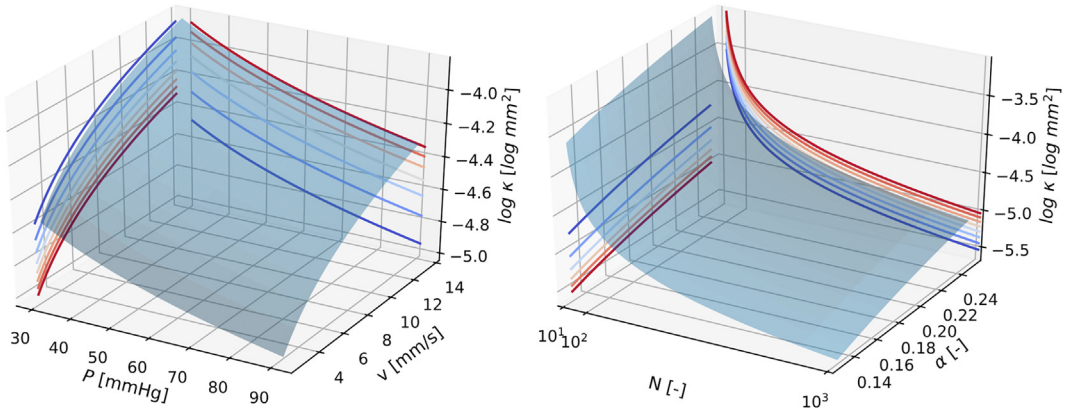

Fig. 6. Thrombus permeability according to Darcy's law and the channel-like thrombus model. Left: decimal logarithm of thrombus permeability, log κ [log mm^2], as a function of typical velocities measured on dynamic CTA, v [cm/s], and realistic values of the pressure drop along the occlusion, ΔP [mmHg], as described by taking the decimal logarithm of Eq. (2). Right: decimal logarithm of thrombus permeability, logκ [log mm^2], as a function of the thrombus void fraction measured on dynamic CTA, α [-], and estimated channel number, N [-], as described by taking the decimal logarithm of Eq. (13).

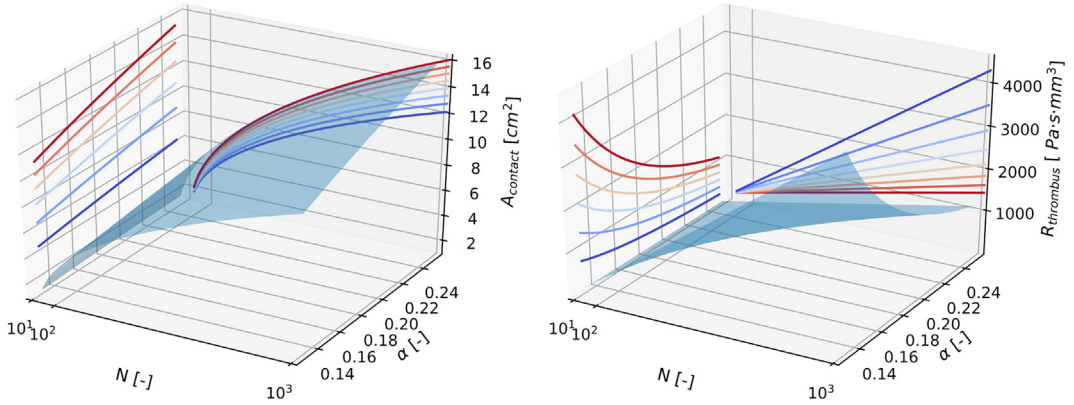

Fig. 7. Thrombus contact area and thrombus resistance. Left: thrombus contact area, $A_{contact}$ [cm^2], as a function of the thrombus void fraction measured on dynamic CTA, α [-], and estimated number of channels, N [-], as described by Eq. (15). Right: thrombus resistance, $R_{thrombus}$ [Pa·s·mm^2], as a function of the thrombus void fraction measured on dynamic CTA, α [-], and estimated number of channels, N [-], as described by Eq. (11).

in dynamic CTA suggests an advective behavior. Therefore, we described permeability based on Darcy's hydraulic conductivity, which is not related to diffusion, concentration gradients, nor Brownian motion, as commonly used in physiology. In the channel-like thrombus model, thrombus permeability is determined by the number of channels, the radius of the occluded artery and the void fraction describing the volume open to the channels and available for the blood to flow. For a given void fraction, more channels within the thrombus imply higher vessel resistance, and therefore less flow through the thrombus, i.e. a reduced permeability. The presented model provides an intuitive way of modeling the relation between thrombus morphology and permeability. This could be of added value in modelling the effects of thrombolytic drugs on a thrombus, where contact surface is relevant.

We introduced the first model that directly quantifies thrombus permeability, and not a derived measure such as perviousness. Perviousness has already been quantified and shown to be related with patient outcome (Santos et al., 2016b, 2016a). Perviousness is a measure reflecting partial information about the porosity and the permeability of the thrombus, since it is quantified at a single

Table 2
Thrombus and blood flow characteristics for patient I, patient II, and the median patient in the study population.

	Patient I	Patient II	Median (IQR)
Thrombus length [cm]	0.69	1.21	1.47 (0.87–1.99)
Thrombus void fraction [-]	0.27	0.06	0.19 (0.13–0.25)
Blood transit-time [s]	0.53	7.55	2.10 (0.78–3.98)
Intra-thrombus blood velocity [cm/s]	1.30	1.16	0.58 (0.26–1.35)
Intra-thrombus blood flow 10^{-3} [ml/s]	13.36	0.38	3.48 (1.71–9.21)

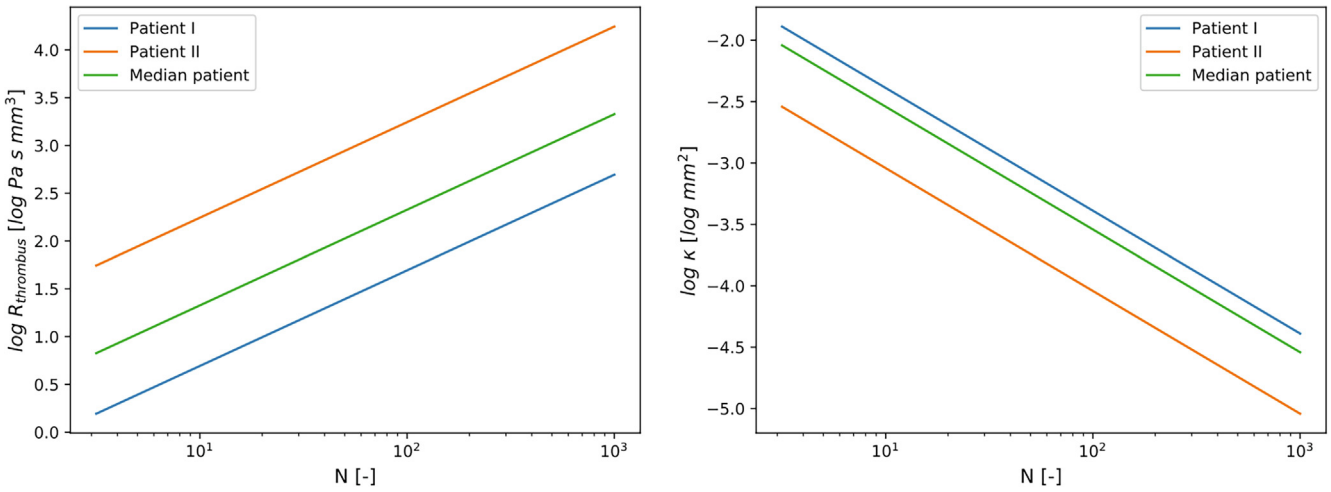

Fig. 8. Thrombus resistance and thrombus permeability according to the channel-like thrombus model. Left: decimal logarithm of thrombus resistance, log $R_{thrombus}$ [log Pa·s·mm^{-3}] as a function of the number of channels, N [-], for patient I, II, and the median patient. Right: decimal logarithm of thrombus permeability, log κ [log mm^2], as a function of the number of channels in the thrombus, N [-], for patient I, II, and the median patient.

instance in time. Perviousness may become a useful measure in daily clinical practice since it can easily be derived from radiological imaging data. However, insight into the dynamics of contrast filling the thrombus, which is a key factor for a better design of thrombolytic drugs, requires understanding permeability.

Thrombus permeability has previously been measured in-vitro on fibrin-gels (Wufsus et al., 2013). The reported permeabilities are lower than the permeabilities in our study (10^{-7}–10^{-10} mm^2 vs. 10^{-3}–10^{-5} mm^2). Wufsus' permeabilities provide velocities orders of magnitude lower than the observed contrast velocities on dynamic CTA data of AIS patients (10^{-3} mm/s vs. 1 mm/s). The permeabilities measured in-vitro in a flow chamber might disregard the in-vivo occlusion pattern. The way the thrombus is obstructing the vessel might allow for channels between the thrombus and the vessel wall, which influences the observed contrast propagation, and therefore, the measured permeability. We should discriminate between the permeability of the thrombus itself (which is probably very low) and the observed permeability due to potential large channels, which would not exist in-vitro.

Our study provides patient-specific information on blood flow characteristics in the vicinity of a thrombus. We showed that the measured velocities within the thrombus were low compared to the centerline velocities in a healthy MCA (40–60 cm/s) (Devault et al., 2008). As a consequence, the intra-thrombus flows were small (blood flow in a healthy MCA (±SD) is 2.43±0.52 ml/s) (Zarrinkoob et al., 2015). Thrombus void fraction has previously been quantified on CTA and NCCT. The reported void fraction values are lower than the ones found in our study, 0.05 (0.01–0.13) vs 0.19 (0.13–0.25) (Santos et al., 2016b). This disagreement might be due to the difference in the used imaging modality (NCCT-CTA vs. dynamic CTA).

The number of channels determines the vessel resistance and the contact area of the blood (contrast, or thrombolytic drug) with the thrombus. This number is difficult to estimate. The variability in thrombus permeability based on the number of channels reflects the difference of having a partially occluding thrombus, i.e. a single large channel, or a group of smaller parallel channels, which strongly increases the resistance. The main goal of the channel-like thrombus model is not to accurately resemble a realistic thrombus morphology, but to provide a simple model able to describe the thrombus resistance, and ultimately, reproduce the flow characteristics observed in dynamic CTA. The real morphology of a permeable thrombus will probably be a more complex structure of tortuous channels and interconnected open spaces.

Permeable thrombi allow the passage of residual flow, which results in anterograde flow distal to the thrombus. Retrograde flow distal to a thrombus, which was also observed, may be a consequence of collateral flow compensating for less permeable thrombi (Liebeskind, 2003). Very permeable thrombi may cause transit-times faster than the timing between the timeframes of the dynamic CTA scan, and therefore, no time delay could be measured.

According to Darcy's law, thrombus permeability establishes a relation between the blood velocities and the pressure drop over the occlusion. This pressure drop depends on the thrombus resistance, the cerebral collateral circulation (Liebeskind, 2003) and the adaptations in downstream vessels, i.e. cerebral autoregulation (Reinhard et al., 2012), which are difficult to quantitate. The chosen range (30–100 mmHg) is expected to cover the range that would lead to clinical symptoms and is based on the only study (as far as we are aware of) that has measured arterial pressure proximal and distal to the thrombus in AIS patients with an intracranial large vessel occlusion (Sorimachi et al., 2011).

Permeability is an important thrombus characteristic. Thrombus permeability may affect the speed at which the infarcted region increases in size. A permeable thrombus allows residual anterograde blood to flow. Residual blood flow can enhance nutri-

tion and oxygen supply to the occluded artery downstream territory, distally from the occlusion. Even a small residual flow may be relevant for the window of treatment. Thrombus permeability, as estimated in our study, will be beneficial for distal perfusion when it allows the passage of RBC and not just plasma and possibly platelets. Nevertheless, the presented permeability model may be of added value in studying the transport of thrombolytic drugs through the thrombus. A thrombus permeability model offers information not only about the remaining flow, but also about the porosity and contact area of the blood with the thrombus. Larger void fraction is translated into more contact area with the thrombus, which may enhance the effect of the drug dissolving the fibrin network.

4.1. Limitations

This study has several limitations. First, the dynamic CTA measurements depend on the placement of the markers, which only sample a certain region, and are observer-dependent (sampling-bias) (Santos et al., 2016c). The main problem encountered by the observers was to define the thrombus-end when distal flow was absent. In these cases, the NCCT scan was used to define the thrombus extension (Dutra et al., 2019). An (semi-)automatized method that extracts the markers from the vessel centerline would be less time-consuming and would reduce the observer-dependency. Second, thrombus length was determined by computing the Euclidean distance between adjacent pair of markers, which is an oversimplification for curved thrombi. Third, no time delay could be measured in some cases due to the fast contrast propagation and the limited temporal resolution of the dynamic CTA scan. Moreover, partial volume effects can have an influence on the density measures of short thrombi with good proximal and distal contrast filling. High contrast intensities proximal and distal to the thrombus may affect the measured contrast intensity within the thrombus, i.e. the measured in-thrombus contrast may be overestimated. This could lead to an overestimation of the thrombus void fraction. Another limitation is that the permeability and the flow characteristics that were extracted/inferred from dynamic CTA reflect the ability of the administered contrast agent to pass through the thrombus. However, this does not imply that RBC, which deliver the oxygen to the tissue and are much larger, are able to pass the occlusion. Additionally, for both the measurements and the model, we considered thrombi as homogeneous. We assumed the flow to be laminar and steady, and blood (and contrast) was assumed to be a Newtonian fluid. Flow propagation was described in the axial direction. However, flow propagation through a porous medium is not trivial, as it will be dictated by the local permeability, which is vectorial. Our focus was not on the microscopic scale of local changes in the flow direction, but rather on the overall flow propagation along the occlusion and therefore, we assumed the flow to be in the axial direction. Finally, for the channel-like thrombus model, the channels were assumed to be straight and all equally wide. It could be interesting to study the effect of curly channels, i.e. longer paths along the thrombus, which would lead to less flow for the same channel number and thrombus void fraction.

5. Conclusion

We have presented a thrombus permeability model in patients with acute ischemic stroke. We have shown that flow in the vicinity of the thrombus is, for all cases, slow. The channel-based thrombus model offers an intuitive way of modelling thrombus permeability, which can be of especial interest in modelling the effect of thrombolytic drugs.

Acknowledgement

This project was funded by the European Union's Horizon 2020 research and innovation programme under grant agreement No 777072 (INSIST project), and the AMC medical Research BV, Amsterdam UMC, location AMC, under project No 21937.

Appendix A: Advection vs. diffusion

The propagation of contrast observed in the dynamic CTA data (which are recorded in a time-lapse of 2 min) suggests an advective transport rather than diffusive. In addition, we computed the Peclet number, defined as

$$Pe = \frac{L_{thrombus}\, v_{blood}}{D_{contrast}}, \tag{20}$$

where $L_{thrombus}$ is the thrombus length, v_{blood} is the intra-thrombus blood (contrast) velocity, and $D_{contrast}$ is the mass diffusion coefficient of contrast. From the measurements performed in dynamic CTA data, we observed that the thrombus length is of the order of 10^{-2} m, and the intra-thrombus blood velocity of the order of 10^{-3} m/s. The contrast agent used in these dynamic CTA scans is Ultravist 300 (Berlex, 2004). The mass diffusion coefficient of this contrast is of the order of 10^{-11} m^2/s (Fontanive, 2010). This gives a Peclet number of 10^6, which implies that advective transport dominates over diffusive transport.

Appendix B: Error quantification

The spatial resolution and temporal resolution are $\Delta x \cdot \Delta y \cdot \Delta z$ = 0.391 mm · 0.391 mm · 0.8 mm, and Δt = 2 s, respectively. The error associated with the computation of the transit-time via cross-correlation function is of the order of half of the inverse of the sampling frequency (Zhang et al., 2013), i.e. ΔTT = 1 s. Using the theory on error propagation, the error of the thrombus length can be computed

$$\begin{aligned}\Delta L &= \sqrt{\left(\frac{\delta L}{\delta x}\right)^2 \Delta x^2 + \left(\frac{\delta L}{\delta y}\right)^2 \Delta y^2 + \left(\frac{\delta L}{\delta z}\right)^2 \Delta z^2} \\ &= \left|\frac{1}{L}\right| \sqrt{(x\Delta x)^2 + (y\Delta y)^2 + (z\Delta z)^2},\end{aligned} \tag{21}$$

where x, y, and z are the distances between adjacent markers along each axis, e.g. $x = x_{i+1} - x_i$. The error in the thrombus length will be ruled by the resolution in the z-direction. The measured thrombus lengths in dynamic CTA are of the order of 10^0 cm. Then, the error in the thrombus length, ΔL, is of the order of 10^{-2} cm.

Similarly, the error in the velocity is given by

$$\Delta v = \sqrt{\left(\frac{\delta v}{\delta L}\right)^2 \Delta L^2 + \left(\frac{\delta v}{\delta TT}\right)^2 \Delta TT^2} = |v| \sqrt{\left(\frac{\Delta L}{L}\right)^2 + \left(\frac{\Delta TT}{TT}\right)^2} \tag{22}$$

The error in the velocity is mainly dictated by the error in the transit-time. The measured transit-times and intra-thrombus velocities in dynamic CTA are of the order of 10^0 s and 10^{-1} cm/s, respectively. Then, the error in the velocity is of the order of Δv 10^{-1} cm/s.

Appendix C: Dependencies on the fixed parameters

When studying thrombus permeability, either through Darcy's equation or through the channel-like thrombus model, we assumed the blood viscosity, the thrombus length, and the MCA radius to be fixed parameters. Here, we studied how these parameters affect thrombus permeability.

Fig. 9 shows the thrombus permeability according to Darcy's law for varying blood viscosity and thrombus length. Blood

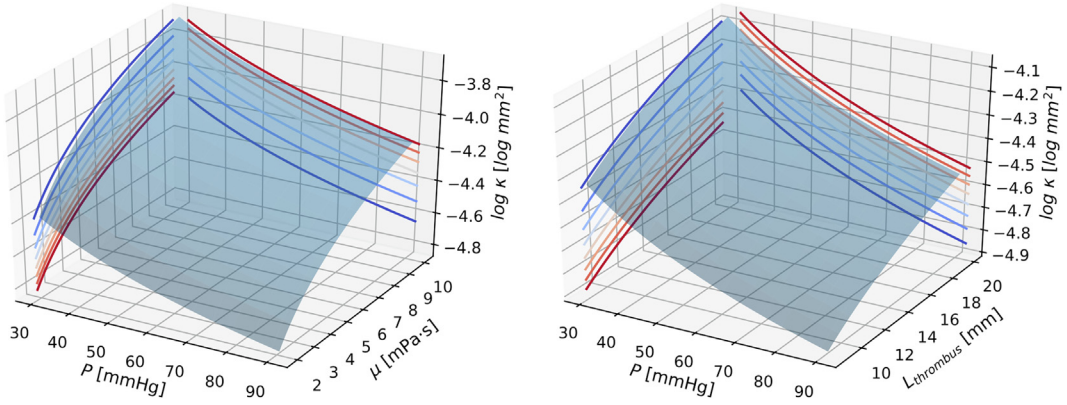

Fig. 9. Thrombus permeability according to Darcy's law for varying blood viscosity and thrombus length. Left: Decimal logarithm of thrombus permeability, log κ [log mm^2], as a function of blood viscosity, μ [mPa·s], and realistic values of the pressure drop along the occlusion, ΔP [mmHg], as described by taking the decimal logarithm of Eq. (2). Right: Decimal logarithm of thrombus permeability, log κ [log mm^2], as a function of thrombus length, $L_{thrombus}$ [mm], and realistic values of the pressure drop along the occlusion, ΔP [mmHg], as described by taking the decimal logarithm of Eq. (2).

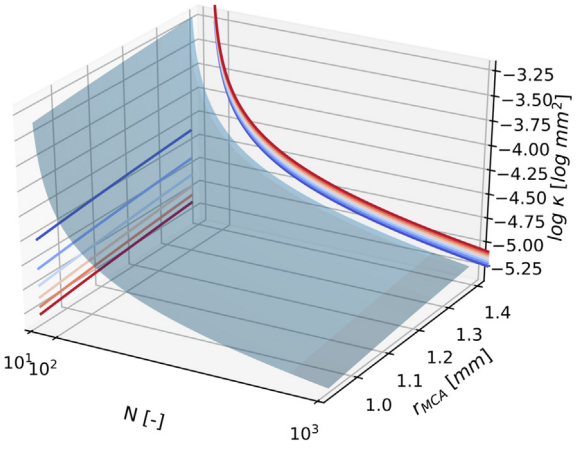

Fig. 10. Thrombus permeability according to the channel-like thrombus model for varying MCA radius. Decimal logarithm of thrombus permeability, logκ [log mm^2], as a function of the MCA radius, r_{MCA} [mm], and estimated channel number, N [-], as described by taking the decimal logarithm of Eq. (13).

viscosity is dependent on parameters such as the haematocrit level or the shear rate. The blood viscosity range displayed in Fig. 9 was taken from (Wells and Merril, 1962). The thrombus length range was based on the measured thrombus lengths on dynamic CTA.

Fig. 10 displays the thrombus permeability according to the channel-like thrombus model for varying MCA radius. The range of MCA radius was taken from (Davison et al., 2018).

Appendix D: Estimation of the number of channels

The number of channels is a parameter of the channel-like thrombus model that needs to be estimated. Our interest is to compare the consequences of having a single large channel (which could be due to the way the thrombus is occluding the vessel, allowing blood to flow between the thrombus and the vessel wall) and having a set of small channels (which would resemble a complete occlusion by a porous/permeable thrombus). The number of small channels is determined based on the dynamic CTA measurements. For the median patient in our population (Table 1), we calculated the permeability based on Darcy's law to estimate the order of number of channels, and the corresponding channel size, using Eqs. (2), (10) and (13). This derivation provides an estimate

Table 3
Thrombus permeability [mm^2], number of channels [-], and channel radius [mm] for the minimum and maximum pressure drops over the occlusion.

	$\Delta P_{thrombus}$=30 mmHg	$\Delta P_{thrombus}$=100 mmHg
Darcy's $\kappa_{thrombus}$ [mm^2]	$6.40 \cdot 10^{-5}$	$1.92 \cdot 10^{-5}$
N [-]	449	1497
R_{ch} [mm]	0.022	0.012

of the number of channels of the order of 10^2–10^3 (Table 3). We therefore set the number of channels from 1 to 1000. The size of these channels (in the order of 10–10^2 μm) would (in theory) allow the passage of RBC, which are around 5 μm in diameter.

References

Bennink, E., Oosterbroek, J., Horsch, A.D., Dankbaar, J.W., et al., 2015. Influence of thin slice reconstruction on CT brain perfusion analysis. PLoS One 10, 1–14.

Berkhemer, O.A., Fransen, P.S.S., Beumer, D., Van Den Berg, L.A., et al., 2015. A randomized trial of intraarterial treatment for acute ischemic stroke. N. Engl. J. Med. 372, 11–20.

Berlex, 2004. Ultravist (brand of iopromide) injection. Berlex NDA 20-220 1–25.

Boeckh-Behrens, T., Schubert, M., Förschler, A., Prothmann, S., et al., 2016. The impact of histological clot composition in embolic stroke. Clin. Neuroradiol. 26, 189–197.

Brass, L.F., Wannemacher, K.M., Ma, P., Stalker, T.J., 2011. Regulating thrombus growth and stability to achieve an optimal response to injury. J. Thromb. Haemost. 9, 66–75.

Carman, P.C., 1939. Permeability of saturated sands, soils and clays. J. Agric. Sci., 29

Davison, M.A., Ouyang, B., Keppetipola, K.M., Chen, M., 2018. Arterial diameter and the gender disparity in stroke thrombectomy outcomes. J. Neurointerv. Surg. 10, 949–952.

De Meyer, S.F., Andersson, T., Baxter, B., Bendszus, M., et al., 2017. Analyses of thrombi in acute ischemic stroke: a consensus statement on current knowledge and future directions. Int. J. Stroke 12, 606–614.

Devault, K., Gremaud, P.A., Novak, V., Olufsen, M.S., et al., 2008. Blood flow in the circle of Willis: modeling and calibration. Multiscale Model Simul. 7, 888–909.

Dutra, B.G., Tolhuisen, M.L., Alves, H.C.B.R., Treurniet, K.M., et al., 2019. Thrombus imaging characteristics and outcomes in acute ischemic stroke patients undergoing endovascular treatment. Stroke, 1–8.

Elert, G., 2019. Viscosity, in: The Physics Hypertextbook.

Fontanive, L., 2010. Nanoscale interaction for higher efficiency of contrast media. PhD thesis Univ. degli Stud. di Trieste.

Frölich, A.M.J., Schrader, D., Klotz, E., Schramm, R., et al., 2013. 4D CT angiography more closely defines intracranial thrombus burden than single-phase CT angiography. Am. J. Neuroradiol. 34, 1908–1913.

Frölich, A.M.J., Wolff, S.L., Psychogios, M.N., Klotz, E., et al., 2014. Time-resolved assessment of collateral flow using 4D CT angiography in large-vessel occlusion stroke. Eur. Radiol. 24, 390–396.

Goyal, M., Menon, B.K., Van Zwam, W.H., Dippel, D.W.J., et al., 2016. Endovascular thrombectomy after large-vessel ischaemic stroke: a meta-analysis of individual patient data from five randomised trials. Lancet 387, 1723–1731.

Gunning, G.M., McArdle, K., Mirza, M., Duffy, S., et al., 2018. Clot friction variation with fibrin content; implications for resistance to thrombectomy. J. Neurointerv. Surg. 10, 34–38.

Jansen, I.G.H., Mulder, M.J.H.L., Goldhoorn, R.J.B., 2018. Endovascular treatment for acute ischaemic stroke in routine clinical practice: prospective, observational cohort study (MR CLEAN Registry). BMJ 360.

Klein, S., Staring, M., Murphy, K., Viergever, M.A., et al., 2010. Elastix : A Toolbox for Intensity-Based Medical Image Registration 29, 196–205.

Kozeny, J., 1927. Ober kapillare Leitung des Wassers im Boden. Akad. Wiss. Wien 136, 271–306.

Liebeskind, D.S., 2003. Collateral circulation. Stroke 34, 2279–2284.

Marder, V.J., Chute, D.J., Starkman, S., Abolian, A.M., et al., 2006. Analysis of thrombi retrieved from cerebral arteries of patients with acute ischemic stroke. Stroke 37, 2086–2093.

Modrau, B., Vestergaard, K., Iversen, H.K., Homburg, A.-M.F., et al., 2007. Thrombolysis for acute ischaemic stroke. Ugeskr. Laeger 169, 3383–3385.

Reinhard, M., Rutsch, S., Hetzel, A., 2012. Cerebral autoregulation in acute ischemic stroke. Perspect. Med. 1–12, 194–197.

Santos, E.M.M., Dankbaar, J.W., Treurniet, K.M., Horsch, A.D., et al., 2016a. Permeable thrombi are associated with higher intravenous recombinant tissue-type plasminogen activator treatment success in patients with acute ischemic stroke. Stroke 47, 2058–2065.

Santos, E.M.M., Marquering, H.A., Den Blanken, M.D., Berkhemer, O.A., et al., 2016b. Thrombus permeability is associated with improved functional outcome and recanalization in patients with ischemic stroke. Stroke 47, 732–741.

Santos, E.M.M., Yoo, A.J., Beenen, L.F., Berkhemer, O.A., et al., 2016c. Observer variability of absolute and relative thrombus density measurements in patients with acute ischemic stroke. Neuroradiology 58, 133–139.

Sorimachi, T., Morita, K., Ito, Y., Fujii, Y., 2011. Blood pressure measurement in the artery proximal and distal to an intra-arterial embolus during thrombolytic therapy. J. Neurointerv. Surg. 3, 43–46.

Van Seeters, T., Biessels, G.J., van der Schaaf, I.C., Dankbaar, J.W., et al., 2014. Prediction of outcome in patients with suspected acute ischaemic stroke with CT perfusion and CT angiography: The Dutch acute stroke trial (DUST) study protocol. BMC Neurol. 14, 1–8.

Wells, R.E., Merril, E.W., 1962. Influence of flow properties of blood upon viscosity-hematocrit relationships. J. Clin. Invest., 41

Wufsus, A.R., MacEra, N.E., Neeves, K.B., 2013. The hydraulic permeability of blood clots as a function of fibrin and platelet density. Biophys. J. 104, 1812–1823.

Zarrinkoob, L., Ambarki, K., Wåhlin, A., Birgander, R., et al., 2015. Blood flow distribution in cerebral arteries. J. Cereb. Blood Flow Metab. 35, 648–654.

Zhang, X., Bai, Y., Chen, X., 2013. An improved cross-correlation velocity measurements method based on fraction delay estimation. Trans. Eng. Technol. (Chapter 10)